

# Improving the Traceable Measurement and Generation of Small Direct Currents

Dietmar Drung, Martin Götz, Eckart Pesel, and Hansjörg Scherer

**Abstract**—We present the latest improvements in the traceable measurement and generation of small electric currents. A central tool in our traceability chain for small direct currents is a new binary cryogenic current comparator (CCC) with a total of 18 276 turns. This 14-bit CCC is well suited for the calibration of high-value resistors and current amplifiers, but also for the direct amplification of small currents. A noise level of  $5 \text{ fA}/\sqrt{\text{Hz}}$  at  $0.05 \text{ Hz}$  is routinely achieved. The systematic uncertainty due to noise rectification was exemplarily investigated in a ratio-error test configuration, showing that a total uncertainty of about one part in  $10^6$  can be achieved at  $100 \text{ pA}$ . For further improvement, a new instrument was developed, the ultrastable low-noise current amplifier (ULCA). Its transfer coefficient is highly stable versus time, temperature, and current amplitude within a full dynamic range of  $\pm 5 \text{ nA}$ . The ULCA is calibrated with the 14-bit CCC at high current amplitude, and allows the measurement or generation of  $100\text{-pA}$  direct current with an uncertainty of one part in  $10^7$ . The novel setup was successfully used to investigate the uncertainty of the established capacitor charging method. A quantum metrology triangle experiment based on the presented instruments is proposed.

**Index Terms**—Ammeters, amplifiers, calibration, instrumentation and measurement, measurement units, noise measurement, superconducting devices, uncertainty.

## I. INTRODUCTION

RECENT advances in the field of single-electron transport (SET) devices offer ways for generating currents of the order of  $100 \text{ pA}$  with uncertainties of one part per million (ppm) or better [1]–[4]. This is expected to have an impact on a future quantum-based realization of the SI unit ampere [5]. Therefore, in the fields of fundamental and practical metrology, the interest in the accurate measurement of small electric currents is growing. Also for application purposes, e.g., in dosimetry and semiconductor industry, there is need for sub-nanoampere current measurements, requiring the calibration of picoamperemeters (picoammeters). In order to underpin their calibration and measurement capabilities in

Manuscript received January 2, 2015; revised March 17, 2015; accepted April 20, 2015. Date of publication June 24, 2015; date of current version October 7, 2015. This work was supported by the Joint Research Project Qu-Ampere within the European Metrology Research Programme (EMRP). The EMRP is jointly funded by the EMRP participating countries within EURAMET and the European Union. The Associate Editor coordinating the review process was Dr. Branislav Djokic.

D. Drung is with Physikalisch-Technische Bundesanstalt, 10587 Berlin, Germany (e-mail: dietmar.drung@ptb.de).

M. Götz, E. Pesel, and H. Scherer are with Physikalisch-Technische Bundesanstalt, 38116 Braunschweig, Germany.

Color versions of one or more of the figures in this paper are available online at <http://ieeexplore.ieee.org>.

Digital Object Identifier 10.1109/TIM.2015.2440564

this field, lately 13 National Metrology Institutes (NMIs) have completed a first international comparison [6].

The traceable generation of sub-nanoampere currents is commonly performed at NMIs with the capacitor charging method or with setups based on applying a voltage to a high-value resistor [6]–[11]. Uncertainties of about 10 ppm are achieved at best [12]; about 1 ppm was reported with a special setup optimized for the measurement of SET devices [1]. This is not sufficient for metrological applications of SET current sources aiming at uncertainties of 0.1 ppm for a  $100\text{-pA}$  output current [13]. For such low uncertainties cryogenic current comparators (CCCs) [14], [15] with a large number of turns were developed that can be used as accurate current amplifiers [16]–[19]. However, the superconducting quantum interference device (SQUID) maintaining zero magnetic flux in the CCC is a strongly nonlinear element. It was recently shown by a simple theoretical example that rectification of wideband noise may cause a systematic error which might increase the overall uncertainty to well above the target value of 0.1 ppm at  $100 \text{ pA}$  [20].

In this paper, a new traceable measurement and calibration setup is presented meeting the ultimate performance requirements of SET devices. In addition, the new method offers significant benefits in handling and operability in comparison with previous setups. This paper starts in Section II with a description of the design and performance of our new 14-bit CCC [19]. In Section III, we exemplarily demonstrate noise rectification effects that limit the uncertainty achievable with the 14-bit CCC to about 1 ppm at  $100 \text{ pA}$ . Section IV deals with the new picoammeter instrument developed at Physikalisch-Technische Bundesanstalt (PTB), the ultrastable low-noise current amplifier (ULCA) [21]. It is shown that 0.1 ppm uncertainty can be achieved with the ULCA after calibration with our 14-bit CCC. In Section V, the new method is compared with the capacitor charging method currently used at PTB for traceable sub-nanoampere current generation. This paper finishes with conclusions in Section VI.

## II. DESIGN AND PERFORMANCE OF PTB'S 14-bit CCC

The 14-bit CCC is a key component in PTB's traceability chain for small direct currents. The recently built CCC torus comprises a total of 20 separate windings (19 accessible at the room temperature interface). In detail, there are windings with numbers of turns as the powers of 2 from 1 to 4096 (the 1- and 1024-turn windings are available twice, and the 4096-turn winding thrice) completed by nonbinary windings with 17, 78, and 773 turns. Two 4096-turn

windings are connected in series within the low-temperature end of the probe thus resulting in an effective 8192-turn winding and finally justifying the denomination as a 14-bit comparator. For reasons not understood so far, one of the two 1024-turn windings has a short to the 2-turn winding when the probe is cooled down, but not at room temperature. As a limitation in operation arising from this defect, these windings cannot be used simultaneously.

The 14-bit CCC probe is as an improved version of its 12-bit predecessor [22], both CCCs are of type I (see [23] for a description of CCC types). The increase in the overall number of turns by roughly a factor of four was compensated for by reducing the wire diameter by a factor of two. The general type of wire was kept (single-filament NbTi in Cu matrix), but the diameter of the conductor was reduced to 25  $\mu\text{m}$  (35  $\mu\text{m}$  including insulation) and the manufacturing becomes disproportionately more challenging. Therefore, the 14-bit CCC could be integrated into a probe for operation in a liquid-helium dewar with a 50-mm neck diameter without compromising the screening (photographs are available in [19]). For the leads between the probe's cold head and its room-temperature electrical interface, we used Teflon-insulated wires with low thermal conductivity. Together with a considerable decrease in the cross section of the supporting stainless steel tubes and with the use of baffles, this helped to reduce the heat load to the helium bath significantly in comparison with the 12-bit CCC probe.

The SQUID's single-turn pick-up loop and the sensor itself are placed in or close to the equatorial plane of the CCC torus, respectively. As previously, a cold  $RC$  damping circuit was applied to reduce the detrimental effect of the CCC's self-resonance. Originally, we intended to use a separate damping winding as in [24], but later we found it more convenient to connect the  $RC$  circuit in parallel to the winding with the highest number of turns (the effective 8192-turn winding). According to the dimensioning rules given in [24], maximizing the number of turns (i.e., the self-inductance) of the winding to which the  $RC$  circuit is connected helps to keep the required capacitance low. We finally selected 2  $\text{k}\Omega$  and 0.9  $\mu\text{F}$  which provides sufficient damping. The original 1024-turn damping winding was made accessible at the room temperature interface (in [19], this was not yet done, which is why 18 windings and a total of 17252 turns were quoted).

The CCC is a dc ratio transformer [14] that is accurate by design; however, deviations from the ideal performance are found as soon as certain design rules are not fulfilled (see [17], [23], and references therein). Fortunately, the ratio error can be made very small by an appropriately large overlap of the screen. The residual ratio error basically represents the dependence of the screening current on the outer surface of the screen on the position of a turn through which an excitation current is flowing, within the entity of the turns in the CCC. Thus, the ratio error has to be understood as a purely geometry-related effect: it is specific to a certain turn with its given position, has to be referred to another turn, and depends on the geometry of the screen. Obviously, for multiturn windings (and combinations of those), the description at the

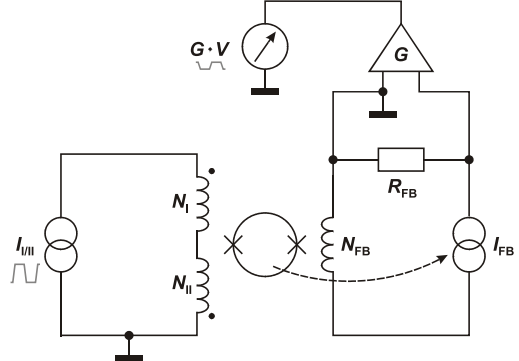


Fig. 1. RET configuration.  $N_I$  and  $N_{II}$  are the equal total numbers of turns of (single or composed) CCC windings connected in series, but having opposite orientation. In case of finite ratio error, the nonzero net flux coupled into the SQUID when a current  $I_{I/II}$  is applied will be cancelled by a feedback flux generated by the current  $I_{FB}$  flowing through another CCC winding with number of turns  $N_{FB}$ . The feedback current is measured via the voltage drop  $V$  across a calibrated resistor  $R_{FB}$ , which is amplified by a factor  $G$  before digitization. For all measurements presented in this paper, we have chosen  $N_{FB} = 1$  and  $R_{FB} = 12.9 \text{ k}\Omega$ . To suppress thermoelectric voltage effects, the direction of  $I_{I/II}$  is periodically reversed, and finally the resulting difference  $\Delta V$  is referred to  $\Delta I_{I/II}$  (symbolically represented as time traces in gray).

single-turn's level becomes inadequate and is better replaced by an integral winding-specific quantity representing the error resulting from contributions of all turns of a winding.

The ratio-error test (RET) is one of the most important steps when characterizing a CCC probe. Besides finding basic faults in the CCC shields (cracks or gaps in the soldering), the purpose of an RET is to obtain a reliable upper limit for the relative deviation of the current ratio fixed by means of the CCC from the inverse ratio of the chosen numbers of turns. Unfortunately, to our knowledge, there exists no commonly agreed procedure for the determination and evaluation of the ratio error (like, e.g., the guidelines [25] for dc measurements of the quantized Hall resistance). At PTB, the RET is performed with the configuration schematically shown in Fig. 1. The instrumentation modules (current sources and amplifier) and measurement software are identical to the ones used in conventional CCC-based resistance calibrations.

As an initial test of the 14-bit CCC, we performed an *overall* RET with  $N_I = N_{II} = 8192$  built from a single winding or composed of 13 windings (with numbers of turns of 4096, 2048, 1024, 512, 256, 128, 64, 32, 17, 8, 4, 2, and 1), respectively. This overall RET is helpful to find basic faults in the CCC construction. The result indicates that the 14-bit CCC meets the quality requirements as well as the established 12-bit CCC does: When biased with  $I_{I/II} = \pm 300 \mu\text{A}$ , the peak-peak error flux  $\Delta\Phi$  was about  $2 \mu\Phi_0$ . This is equivalent to the magnetic flux that would be generated by the given current  $I_{I/II}$  flowing through a  $3.7 \times 10^{-8}$  fraction of a turn; the nominally identical  $N_I$  and  $N_{II}$  of 8192 effectively differ by  $\Delta N_{I/II} = 3.7 \times 10^{-8}$  corresponding to a relative deviation  $\Delta N_{I/II}/N_I$  of 4.5 parts in  $10^{12}$ . Note that the overall RET does not replace a detailed validation where each winding is checked separately by a series of build-up tests (1:1, 2:2, 4:4, etc.), because the contribution of the low-turn windings is small in an over-

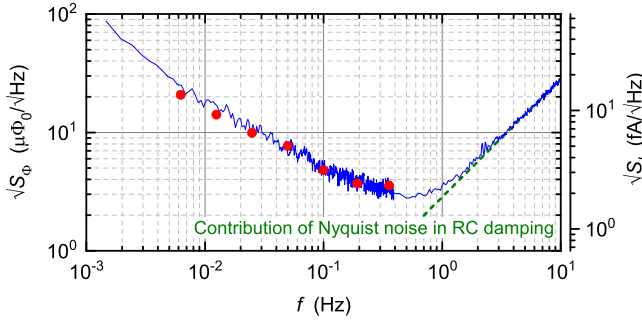


Fig. 2. Low-frequency flux noise spectrum of the SQUID mounted in the 14-bit CCC. The noise was recorded with an Agilent 35670A dynamic signal analyzer. The current noise scale on the right-hand side was calculated from the measured flux linkage sensitivity of 11.1 microamp-turns per  $\Phi_0$  by assuming an input coil with 17000 turns. The red data points are deduced from  $\tau^{-1/2}$  fits of the Allan deviation data shown in Fig. 3. The dashed line shows the contribution calculated from Nyquist noise in the cold *RC* damping circuit.

all test. For example, the above-mentioned overall deviation of  $3.7 \times 10^{-8}$  turns would be unacceptable if it were caused by a winding with a few turns only.

A first flux noise spectrum of the mounted SQUID in the frequency range up to 100 kHz has already been presented in [19], with the damped self-resonance of the CCC found at about 200 Hz and a flux noise below  $4 \mu\Phi_0/\sqrt{\text{Hz}}$  in the frequency range from about 0.2 to 1 Hz ( $\Phi_0$  denotes the flux quantum of 2.07 fWb). The relatively low resonance frequency of 200 Hz results from the increased winding inductance compared with the 12-bit CCC and extra stray capacitance in the wiring. In a later cool-down, we recorded the flux-noise spectrum shown in Fig. 2 with the focus on lower frequencies (down to about 1 mHz) which is the relevant range for CCC measurements. We found excellent agreement with the older data. The increase in noise above about 1 Hz is caused by Nyquist noise in the *RC* damping circuit as shown in Fig. 2 by the calculated dashed line. This excess high-frequency noise is not an issue in practice because the currents in dc measurements are typically reversed with a repetition frequency  $f_R$  well below 1 Hz to suppress settling effects after current reversal.

In practical CCC applications, we observe that the noise figure is deteriorated by strong electric distortions exceeding those during normal CCC operation substantially. This occurs, e.g., when connecting resistors to the CCC windings or changing the ranges of the double-current source in our measurement bridge. However, heating the SQUID chip for 0.1 s (heater integrated on-chip) is always sufficient for restoring the favorable performance shown in Fig. 2.

The noise spectrum in [19] was measured without connections to the CCC windings. This passive condition differs from that of CCC operation, e.g., as a part of a measurement bridge for resistance calibration. Here, current sources (with low, but non-negligible noise) and resistors (introducing thermal noise) are connected to the windings. In addition, electromagnetic distortions (for example, picked up along the leads connecting the resistors to be compared) can be coupled into the SQUID sensor. Furthermore, the currents through the windings are periodically reversed in order to suppress low-frequency noise and drift effects.

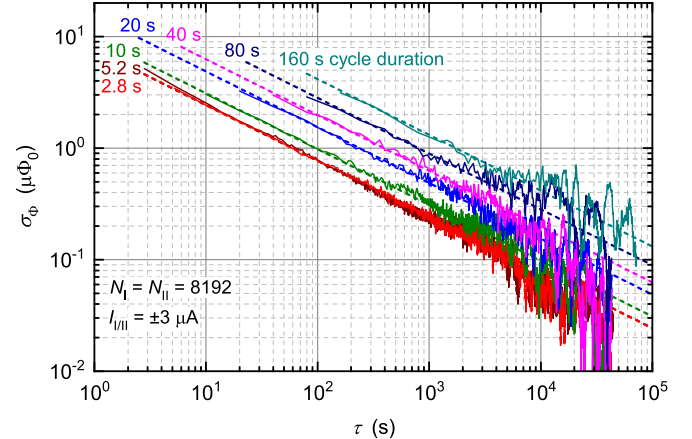


Fig. 3. Allan deviation plot of an RET with  $N_I = N_{II} = 8192$  and  $I_{I/II} = \pm 3 \mu\text{A}$  (in  $\pm 300 \mu\text{A}$  range). Seven cycle durations between 2.8 and 160 s were chosen; the two shortest (2.8 and 5.2 s) yield almost identical results indistinguishable in the diagram. The current is reversed twice per cycle, and the first half of the data points at each current level is disregarded to suppress settling effects. The slope of the dashed lines corresponds to a  $\tau^{-1/2}$  dependence. From their respective vertical position in the plot, the red dots in Fig. 2 have been calculated.

To demonstrate the noise performance under real operation conditions, a series of RET measurements was performed and the noise level was analyzed. Our standard current reversal setting is a full cycle time of 20 s, i.e., two 10-s half cycles, each including 0.2 s for ramping and a 9.8-s plateau time. As the cycle duration will strongly affect the type A uncertainty according to the low-frequency excess noise seen in Fig. 2, cycle durations from 2.8 up to 160 s were investigated [26]. The corresponding Allan deviation plots are shown in Fig. 3. From the predominant  $\tau^{-1/2}$  dependence of the Allan deviation  $\sigma_\Phi$  on the sampling time  $\tau$ , one can conclude that, even at the scale of hours, there is no significant distortion of the measurements by drifts, i.e., an increase in the measurement time will still result in a lower type A uncertainty. For our standard cycle duration of 20 s, the type A standard uncertainties of RET measurements are typically about 0.25 or 0.05  $\mu\Phi_0$  for an averaging time of 1 h or one day, respectively. The respective SQUID noise can be deduced from the vertical position of the curves in these plots. According to [21], we calculated the corresponding flux noise levels and included them as red dots in Fig. 2. Good agreement with the SQUID's noise spectrum was found. Note that the low-frequency noise in Fig. 2 (recorded in the RET configuration with the current sources connected to the windings, but at zero current) is consistent with the intrinsic noise of the SQUID. Therefore, we conclude that the sensor's noise figure is not compromised in a resistance comparison measurement.

### III. LIMITATIONS FROM NOISE RECTIFICATION

Within the report on the 2013 onsite comparison in resistance measurements of Bureau International des Poids et Mesures (BIPM) and PTB [27], we have recently summarized the results of a comprehensive RET series for the 12-bit CCC. There we pointed to the difficulty that besides the geometry-related effect discussed

above, mixing-down or noise rectification effects in the SQUID, a nonlinear detector, contribute to RET measurement results. In this section we will describe a new experimental study of how strong mixing-down can influence RET results as well as those of any other measurement with the given 14-bit CCC plus SQUID combination.

We start with the assumption that the geometry-related ratio error discussed in Section II will be dominant for high amp-turn products  $\Delta I_{\text{I/II}} N_{\text{I}} = \Delta I_{\text{I/II}} N_{\text{II}}$  (high-flux regime) and the mixing-down effect for low ones (low-flux regime)—provided that the wideband noise level is constant. In more detail, for the geometry-related ratio error resulting from the position-dependent mutual inductance contributions of the turns, one expects a strictly linear relation between  $\Delta I_{\text{I/II}}$  and  $\Delta V$  (see Fig. 1). When considering this case alone, the calculated  $\Delta N_{\text{I/II}}$  will not depend on  $\Delta I_{\text{I/II}}$ . Different from that, rectified wideband noise depends nonlinearly on the noise amplitude, but provides a constant contribution to  $\Delta V$  as long as the noise level does not change.

This constant noise level is a key assumption in our experimental approach. We varied the  $I_{\text{I/II}}$  amplitude by a factor 100, but kept the  $I_{\text{I/II}}$  range constant ( $\pm 300 \mu\text{A}$ ) because the wideband current noise of our source module is known to increase with the current range (nine different ranges from  $\pm 5 \mu\text{A}$  up to  $\pm 300 \text{ mA}$  can be selected), but to be practically independent of the chosen amplitude within a given range. As an example, in one experiment  $\Delta\Phi$  changed from about  $2 \mu\Phi_0$  at  $\pm 300 \mu\text{A}$  to  $-0.4 \mu\Phi_0$  at  $\pm 3 \mu\text{A}$ , corresponding to ratio errors of 4.5 or  $-90$  parts in  $10^{12}$ , respectively. The geometry-related error can be determined from the difference between the two measurements: the difference in flux of  $2.4 \mu\Phi_0$  caused by the difference in current of  $\pm 297 \mu\text{A}$  yields a geometry-related ratio error of 5.5 parts in  $10^{12}$ . The ratio error in the low-flux regime as resulting from the superposition of geometry and mixing-down effects is about 16 times larger and of reverse sign than the geometry-related effect. This clearly indicates how crucial mixing-down of noise can become under low-flux conditions and that this effect generally has to be considered.

For learning more about mixing-down in the low-flux regime, we have varied the noise level as well as we have manipulated the mixing-down mechanism. The RET experiments reported so far in this paper have been performed in a configuration wherein the chargers for the current source modules as well as those for the central processing unit and the bridge instrument have been active. The several chargers are significant sources of high-frequency noise as can easily be observed by displaying the SQUID voltage-flux characteristic with a high bandwidth. The dc-dc converters of the chargers operate at about 180 kHz, which is much higher than the bandwidth of the external feedback loop, but well within the bandwidth of the internal wideband feedback that increases the SQUID's dynamic range [22], [24]. The interference becomes stronger when the number of connected turns of the CCC is increased—exactly this situation we have here with the very high numbers  $N_{\text{I}} = N_{\text{II}} = 8192$  resulting in a peak-peak interference of about  $\Phi_0/3$  (corresponding to 450 pA in a 8192-turn winding). However, for about 20 h, the current

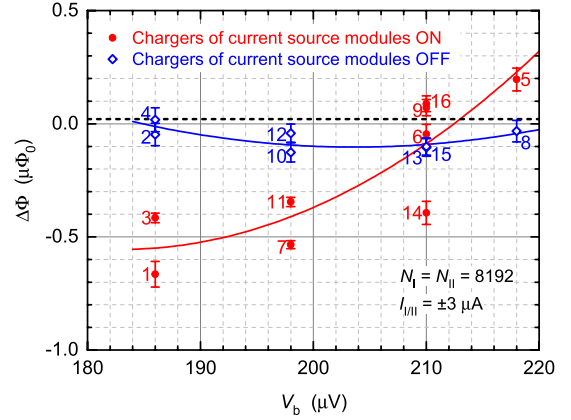


Fig. 4. Peak-peak error flux  $\Delta\Phi$  as a function of the SQUID bias voltage  $V_b$  for RETs in the low-flux regime ( $I_{\text{I/II}} = \pm 3 \mu\text{A}$ ). Error bars indicate type A standard uncertainties. A series of 16 measurements was performed over a period of 44 days. The individual results are labeled according to the order of the measurements in time and the dashed horizontal line indicates the estimated contribution of the geometry-related ratio error for the given flux level. Quadratic polynomial fits (solid lines) serve as guides for the eye.

sources can be operated in battery-powered mode, i.e., the corresponding chargers can be switched OFF temporarily. Taking advantage of this option, we compare the low-flux RET results for two significantly different noise situations as obtained for the current source module chargers being switched ON or OFF, respectively. Note, that the other chargers (for the central unit and for the bridge instrument) have been kept running; the digital communication for data acquisition etc. cannot be switched OFF anyway.

The mixing-down effect depends strongly on the working point of the SQUID's voltage-flux characteristic [28]. One of the relevant bias parameters in our two-stage SQUID sensor is the bias voltage  $V_b$  of the output SQUID array [29]. We manipulated the mixing-down effect by changing  $V_b$  from the original setting of  $186 \mu\text{V}$  while all other SQUID settings were kept unchanged. In Fig. 4, we present a series of RET measurements showing the dependence of the error flux  $\Delta\Phi$  on the bias voltage  $V_b$  and the charger state of the current source modules. The duration of any RET represented in this plot is 18 h, except for a few considerably longer as can be seen from the correspondingly reduced type A uncertainty. Altogether, the results indicate the following tendencies.

- 1) The reproducibility of RET results is better for the measurements with the chargers switched OFF than for those when switched ON.
- 2) The magnitude of the error flux  $\Delta\Phi$  is typically smaller when the chargers are switched OFF—this is exactly what one would expect when reducing the noise level. However, a slight dependence on  $V_b$  seems to remain even for the favorable OFF-state.
- 3) The original working point of the SQUID ( $V_b = 186 \mu\text{V}$ ) appears to be less robust with respect to noise rectification than the working point  $V_b = 210 \mu\text{V}$  identified within this series of measurements and thereafter set as default. All measurements presented in this paper are obtained with  $V_b = 210 \mu\text{V}$  unless otherwise noted.

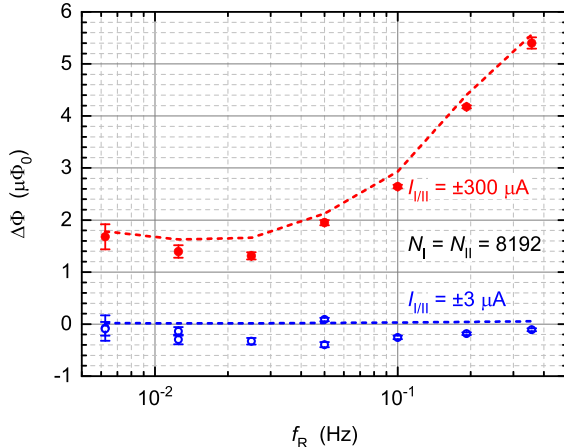


Fig. 5. Peak-peak error flux  $\Delta\Phi$  as a function of repetition frequency  $f_R$  in the high-flux regime (full red circles) and low-flux regime (open blue circles), respectively. Dashed lines show the geometry-related ratio error calculated from the measured difference in  $\Delta\Phi$  between low-flux and high-flux regimes. Error bars indicate type A standard uncertainties. A series of 17 measurements was performed over a period of 22 days. The averaging time for each measurement was one day [for  $f_R = 0.36$  Hz and  $I_{VII} = \pm 300 \mu\text{A}$  it was reduced to 1½ h due to the limited availability of the CCC system]. The chargers in the current source modules were turned ON, and the SQUID bias voltage was set to  $V_b = 210 \mu\text{V}$ .

- 4) The nonlinear effects are not stable enough to be corrected for by calibration.

Changing the charger state in the current source modules at  $V_b = 186 \mu\text{V}$ , we observed a dc shift in the SQUID output of about  $500 \mu\Phi_0$ . In this configuration, the magnitude of the dc shift caused by rectification was about 0.15% of the peak-peak amplitude of the charger interference, and the magnitude of the resulting peak-peak error flux (i.e., the change in the dc shift for positive and negative polarities of  $I_{VII}$ ) was about 0.1% of the magnitude of the dc shift. The dc shift nearly vanished around  $V_b = 218 \mu\text{V}$ , indicating minimum sensitivity to the charger interference at this SQUID bias point. Unfortunately, the minimum was not stable in time, which explains the large scatter of the data points observed in Fig. 4 with the chargers turned ON. Note that for the bias voltage range in Fig. 4, the measured noise levels were not noticeably dependent on the charger state (the noise measurements in Section II were actually done with the chargers turned ON). Although degradation in noise should occur when the SQUID is exposed to a very strong high-frequency interference, at the level caused by the chargers in our CCC electronics we do not observe a correlation between the low-frequency noise level and the error caused by noise rectification. This is a severe obstacle in practice, as a normal noise level does not guarantee sufficiently low systematic errors.

The frequency dependence of the error flux on the repetition frequency  $f_R$  (i.e., the inverse cycle duration) was also investigated for the chargers turned ON. Fig. 5 depicts the results for the high-flux and low-flux regimes, respectively. The dashed lines show the dependence of the geometry-related errors; the deviations from these lines are caused by rectification effects. In the high-flux regime, the nonlinear errors are small compared with the geometry-related ones, but in the low-flux regime they are dominant. At the highest repetition frequency

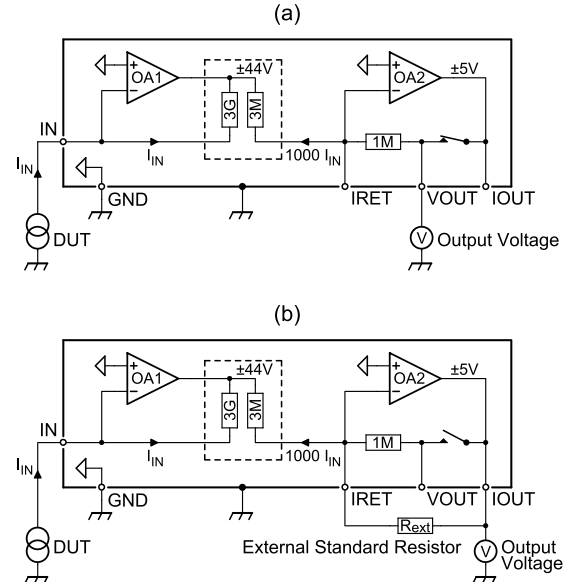


Fig. 6. Basic schematics of the ULCA with (a) voltage output and (b) current output. The input current  $I_{IN}$  is amplified 1000 times by operational amplifier OA1 and a 3-GΩ/3-MΩ resistor network. The output stage OA2 converts the amplified current into a voltage via the internal 1-MΩ reference resistor (voltage output) or an external standard resistor  $R_{ext}$  (current output), respectively. The output voltage range is  $\pm 44$  V for OA1 and  $\pm 5$  V for OA2. The internal reference potential (open triangles) is connected to the ULCA's metal housing via a short on the GND connector.

$f_R = 0.36$  Hz, the geometry-related ratio error amounts to 12.5 parts in  $10^{12}$  ( $\Delta N_{VII} \approx 10^{-7}$ ).

As a preliminary conclusion, we point out that nonlinear effects exist and affect experimental results in the low-flux regime. An influence of the way how combined windings are composed by order (not varied here) is known from earlier CCC experiments and even dependence on the liquid-helium filling level or on the initial charging state of the battery cannot be excluded. In other words, even in the case of an intensively studied CCC plus SQUID probe as the one considered here, there remains an uncertainty span which (expressed in units of magnetic flux) is of the order of  $0.1 \mu\Phi_0$  for the battery-powered, or nearly  $1 \mu\Phi_0$  for the charging mode. Note that for a dc current of  $100 \text{ pA}$ , an uncertainty in flux of  $0.1 \mu\Phi_0$  corresponds to a relative uncertainty of 0.65 ppm. Thus, we conclude that with our 14-bit CCC setup overall uncertainties of the order of 1 ppm can be achieved at  $100 \text{ pA}$ .

#### IV. DESIGN AND PERFORMANCE OF THE ULCA

To reduce the achievable uncertainty at small currents even further, the ULCA concept was developed [20], [21]. The main idea is to combine the excellent low-frequency noise performance of semiconductor current amplifiers with the absolute accuracy of the CCC: the amplifier is utilized for the *measurement* of the small current, but the CCC is used for the amplifier's *calibration* at high current levels where the effect of noise rectification is sufficiently low. Prerequisite is, however, that the amplifier exhibits sufficient stability and linearity.

The ULCA is schematically illustrated in Fig. 6. It consists of two stages, the first providing a 1000-fold amplification of the current  $I_{IN}$  from a device under test (DUT) and the second performing a current-to-voltage conversion. The operational amplifiers OA1 and OA2 in Fig. 6 are sophisticated

circuits comprising several monolithic op amps. This results in a very high overall open-loop gain  $\gg 10^9$  and a correspondingly low input resistance of the order of  $1\ \Omega$ . A very low input current noise of  $2.4\text{ fA}/\sqrt{\text{Hz}}$  is achieved with an onset of low-frequency excess noise at about  $1\text{ mHz}$ . The ULCA's noise level is lower than that of the 14-bit CCC for frequencies below about  $0.2\text{ Hz}$ .

In normal operation, the ULCA effectively acts as a current-to-voltage converter. Its overall transresistance is  $A_{TR} = G_I R_{IV}$ , where  $G_I = 1000$  is the current gain of the input stage and  $R_{IV}$  is the current-to-voltage coefficient of the output stage. The latter is practically equal to the feedback resistance of the output stage thanks to the high open-loop gain of OA2. In voltage output mode, the internal  $1\text{-M}\Omega$  resistor is used for feedback, yielding  $A_{TR} = 1\text{ G}\Omega$ . In current output mode, an external standard resistor  $R_{ext}$  is applied. With the actual amplifier design,  $R_{ext}$  can be chosen between a short (for example, a CCC winding during calibration [21]) and  $100\text{ M}\Omega$ . This way, the transresistance can be increased up to  $100\text{ G}\Omega$ , or the performance can be improved if the quality of the external standard resistor exceeds that of the internal  $1\text{-M}\Omega$  metal-foil resistor. Note that the ULCA can also be configured for current sourcing or for the calibration of high-value resistors [21]; here, the same accuracy is achieved as for current amplification.

The achievable calibration uncertainty of the current gain  $G_I$  is directly affected by nonlinear effects in the  $3\text{-G}\Omega/3\text{-M}\Omega$  resistor network (an array of about 3000 discrete  $2\text{-M}\Omega$  chip resistors). Therefore, the 14-bit CCC was used to experimentally evaluate an upper limit for the resistor nonlinearity. Linearity measurements are sensitive to slow gain fluctuations and drift due to the long averaging times required for achieving a  $<0.1\text{ ppm}$  accuracy at low input currents. To minimize these effects, a special measurement sequence was applied. Instead of measuring the data points of a diagram successively (each with a long averaging time), short sampling times were used and the whole procedure was repeated until sufficient averaging effect was obtained for each point. This way, very long averaging times can be realized without suffering from slow gain fluctuations and drift. Due to the high degree of utilization of the CCC resistance bridge, the measurement had been limited to about one day, yielding information at  $0.1\text{ ppm}$  level only.

The gain nonlinearity  $\Delta G_{NL}$  is defined here as the difference between the measured current gain  $G_I$  and the mean value for all data points of the respective diagram. Two representative cases are presented in Fig. 7. Panel (a) of Fig. 7 shows the gain nonlinearity  $\Delta G_{NL}$  versus the peak amplitude  $I_P$  with zero offset current  $I_0 = 0$  (i.e., the current was switched between  $\pm I_P$ ), whereas panel (b) of Fig. 7 depicts the dependence of  $\Delta G_{NL}$  on an intentionally applied offset current  $I_0$  for fixed amplitude  $I_P = 3.2\text{ nA}$ . Within the random uncertainty, no clear dependence is visible at  $0.1\text{ ppm}$  level, consistent with a voltage coefficient of  $<0.1\text{ ppm/V}$  expected for high-quality thin-film resistors.

The ULCA is calibrated in two steps with the setup shown in [21, Fig. 11]. In the first step, the current gain  $G_I$  of the input stage is calibrated with the CCC alone, i.e., without

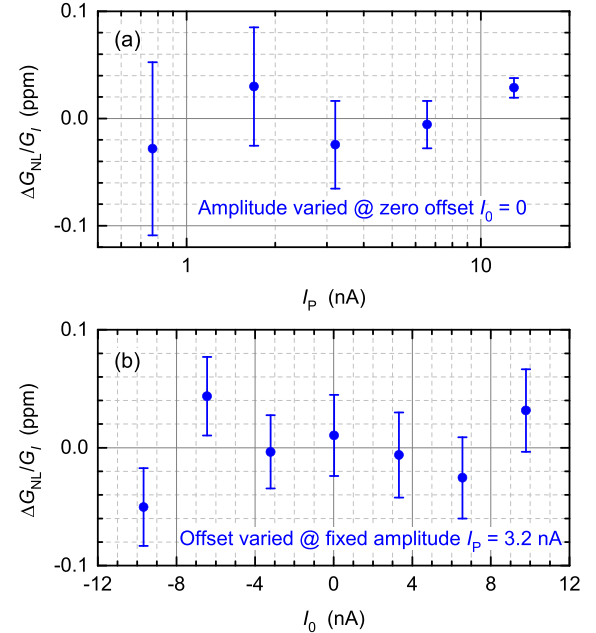


Fig. 7. Relative nonlinearity  $\Delta G_{NL}/G_I$  of the current gain measured with the 14-bit CCC (a) versus peak amplitude  $I_P$  for zero offset  $I_0 = 0$  and (b) versus offset current  $I_0$  for fixed amplitude  $I_P = 3.2\text{ nA}$ . The setup depicted in [21, Fig. 11(a)] was used. The current was reversed every  $10\text{ s}$ , and the first  $2\text{ s}$  after each reversal were disregarded. Error bars indicate type A standard uncertainties. In (a), each data point was derived from five short measurements with 24 full current cycles (48 cycles for  $I_P = 1.7\text{ nA}$  and 96 cycles for  $I_P = 0.77\text{ nA}$ ) resulting in a total averaging time of  $6\text{ h}$ . In (b), each data point was derived from six short measurements with 24 full current cycles yielding a total averaging time of about  $5\frac{1}{2}\text{ h}$ .

TABLE I  
UNCERTAINTY BUDGET FOR THE CALIBRATION  
OF THE  $3\text{-G}\Omega$  INPUT STAGE

Component	Distribution	Comment	Uncertainty (ppm)
Noise	Normal	$\tau \approx 3600\text{ s}$	0.03 (0.045)
Settling	Rectangular	$1/t$ dependence with $<0.1\text{ ppm}$ after $2\text{ s}$	0.016
SQUID nonlinearity	Rectangular	$ \Delta\phi  < 1\ \mu\Phi_0$	0.015 (0.06)
Resistor nonlinearity	Rectangular	Voltage coefficient $<0.1\text{ ppm/V}$	0.047
CCC bridge	Rectangular		0.003
Total			0.06 (0.09)

The quoted uncertainties are standard uncertainties (coverage factor  $k = 1$ ) obtained with the 14-bit CCC; values for the 12-bit CCC are given in parentheses if they differ from those for the 14-bit CCC.

involving an external standard resistor. This calibration is done using CCC windings with a turn ratio of 16000:16 and currents of  $\pm 13\text{ nA}$  and  $\pm 13\text{ }\mu\text{A}$ , respectively. In the second step, the transresistance of the output stage ( $R_{IV} = 1\text{ M}\Omega$ ) is calibrated against a  $12.9\text{-k}\Omega$  standard resistor with a turn ratio of 4029:52 and currents of  $\pm 500\text{ nA}$  and  $\pm 38.74\text{ }\mu\text{A}$ , respectively. For highest accuracy, the quantum Hall resistance (QHR) might be directly used instead of a calibrated standard resistor.

Table I summarizes the uncertainty contributions of the input stage calibration. The noise component includes noise

from the bridge voltage detector and short-term fluctuations of the current gain. For the settling component, slowly decaying transients with a time dependence near  $1/t$  are relevant only [26], [30]; exponential terms are negligible because the respective time constants are low and the first 5 s after each current reversal are typically disregarded (time counted relative to the start point of the 0.2-s current ramp). As a conservative limit, a  $1/t$  dependence with a maximum deviation of 0.1 ppm after 2 s is assumed. The effect of SQUID nonlinearity is taken into account by an error flux  $\Delta\Phi$  equally distributed in the range between  $\pm 1 \mu\Phi_0$ . Nonlinearity of the NiCr thin-film resistors also has to be considered (amplifier effects can be neglected because of the high open-loop gain  $\gg 10^9$ ). The assumed voltage coefficient of  $<0.1$  ppm/V yields an uncertainty contribution of 0.047 ppm for the voltage drop of 0.81 V across the 2-M $\Omega$  resistors of the low-ohmic side of the 3-G $\Omega$ /3-M $\Omega$  resistor network during calibration. The CCC bridge contribution summarizes all systematic uncertainties related to the experimental setup, e.g., the gain error of the bridge voltage detector and the ratio errors of the CCC windings and the binary compensation unit [31].

For the input stage calibration with 14-bit CCC, a total standard uncertainty of 0.06 ppm is achieved. With the 12-bit CCC, the uncertainty contributions from noise and SQUID nonlinearity are higher (values in parentheses in Table I) because of the lower number of CCC turns (4000:4 instead of 16 000:16). This increases the total uncertainty to 0.09 ppm. The calibration uncertainty of the output stage is similar to that of a 1-M $\Omega$  standard resistor, yielding a value of about 0.01 ppm both with the 12-bit and with the 14-bit CCC.

## V. VERIFICATION OF PTB's CAPACITOR CHARGING SETUP

At around 100 pA, the achievable uncertainty of the new instruments ULCA and 14-bit CCC is substantially lower than that of the capacitor charging method currently used at PTB for picoammeter calibrations. To verify the quoted uncertainty of our setup, in particular, the effect of the capacitor's frequency dependence [32], the transresistance  $A_{TR}$  of a ULCA was—for comparison—calibrated both with the capacitor charging setup and with the 14-bit CCC. Preliminary results are reported in [33]. However, these measurements were performed with a ULCA prototype having a lower transresistance of 50 M $\Omega$  and a less accurate calibration than the final instrument used for the measurements presented in this paper.

The CCC calibrations were carried out with the setup shown in [21, Fig. 11] directly before and after the calibrations with the capacitor charging method (see Fig. 8). The drift of  $A_{TR}$  determined from the CCC calibrations was about six parts in  $10^7$  over the complete measurement time of six days. Note that the ULCA prototype used in this experiment showed an exceptionally high drift; devices fabricated later on showed a typical drift of about one part in  $10^7$  over a six-day period.

For the capacitor charging method we used a digital voltage ramp generator that is capable of generating voltage ramps running between  $-10$  and  $+10$  V with a highly stable and

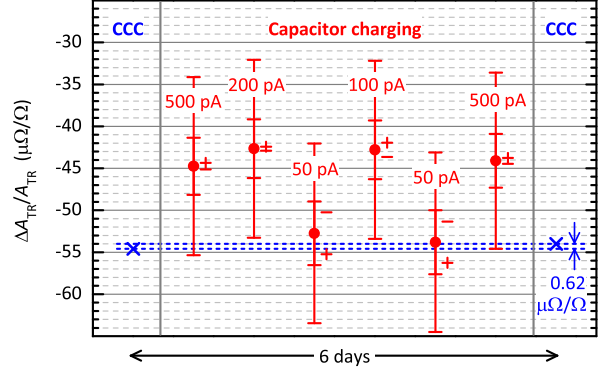


Fig. 8. Comparison of the two ULCA calibration methods with CCC (blue crosses) and via capacitor charging (red dots). Each red dot represents the average of the values for positive and negative current directions, indicated by plus and minus symbols, respectively. The plot shows the relative deviations of the ULCA transresistance from the nominal value (23 °C reference temperature). The data are plotted in the chronological order of the measurements. For the capacitor charging method, standard uncertainties are shown without (small red bars) and with (larger red bars) the contribution of  $10 \mu\Omega/\Omega$  due to the frequency dependence of the capacitance. The uncertainty from the CCC calibrations of  $0.06 \mu\Omega/\Omega$  is not visible in the plot.

linear slope, adjustable between  $\pm 1$  mV/s and  $\pm 1$  V/s [34]. The ramp generator output was monitored using a calibrated 8½-digit multimeter, triggered by a stabilized precision time base. The ramp generator output was connected to one electrode of a commercial capacitor of type GR1404 with nominal capacitance  $C = 1$  nF, calibrated with a commercial precision capacitance bridge at 1 kHz. The other electrode was connected to the ULCA input via a low-noise coaxial cable, and the resulting ULCA output voltage was sampled by another calibrated 8½-digit multimeter. Calibration currents between  $\pm 50$  and  $\pm 500$  pA were applied in subsequent cycles, each of them consisting of the four phases: 1) zero current; 2) positive current; 3) zero current; and 4) negative current. The duration of each phase ranged between 40 and 200 s. Data acquisition was performed over periods between 8 and 66 h of duration, depending on the current value. The statistical uncertainty typically was about  $2 \mu\Omega/\Omega$  or below.

Fig. 8 shows the results of the eight calibrations in chronological order. The relative deviations of the ULCA transresistance from the nominal value were referred to 23 °C by means of the ULCA's internal temperature sensor [21]. The values obtained with the capacitor charging method were higher than the CCC results, typically by about  $10 \mu\Omega/\Omega$  for  $\pm 100$  to  $\pm 500$  pA, but less than  $2 \mu\Omega/\Omega$  for  $\pm 50$  pA. The discrepancy between  $\pm 50$  pA and the other current levels was reproduced by repeating the  $\pm 50$  pA measurement. In both calibrations with  $\pm 50$  pA, the  $A_{TR}$  values exhibited significant and reproducible differences for positive and negative current directions (indicated in Fig. 8 by plus and minus symbols). Although the deviations found in the measurement runs at  $\pm 50$  pA have not been understood yet and are subject of ongoing investigations, we attribute them to the current generation. This assumption is supported by results of a ULCA self-test, i.e., a configuration where the current gains of two ULCA channels are directly compared against each other without a CCC [21]. With this setup, a reduction of the current level from  $\pm 3.3$  nA to  $\pm 50$  pA resulted in a gain change of about 1 ppm;

however, the standard uncertainty at  $\pm 50$  pA also was about 1 ppm. Note that for high currents the measured relative gain in the self-test agreed within about 0.1 ppm with CCC calibrations performed shortly before and after the self-test.

The effect of the frequency dependence of the capacitance was investigated in [32], in particular also that of the specimen used for the measurements shown in Fig. 8. The capacitance increased by 5–10  $\mu\text{F}/\text{F}$  (however, with an uncertainty of about 10  $\mu\text{F}/\text{F}$ ) when the measuring frequency was lowered from the 1 kHz operation frequency of the capacitance bridge used for the capacitor calibration down to the range of millihertz frequencies (i.e., the effectively relevant voltage ramp frequencies for the capacitor charging method). The observation that the  $A_{TR}$  values determined with the capacitor charging method are larger than the CCC results is consistent with the findings in [32]: an effectively larger capacitance at dc yields a current that is larger than nominally assumed. This current, when fed into the ULCA input, will result in a larger output voltage and, thus, a larger calibration value for  $A_{TR}$ .

## VI. CONCLUSION

We have presented a 14-bit CCC with the lowest noise level reported so far for frequencies below 0.4 Hz (our frequency range of interest). The device is highly suited for demanding applications in fundamental research where the current resolution of a 12-bit CCC is no more adequate. Our 14-bit CCC offers valuable advantages in low-current experiments. The achievable uncertainty at 100 pA (the typical output of an SET device) is about 1 ppm. It is limited by rectification of wideband noise in the SQUID which was demonstrated and quantitatively investigated during RETs. We consider noise rectification as a general and severe obstacle in the approach of operating a CCC with a high number of turns as a precise amplifier for sub-nanoampere currents. In principle, the nonlinearity could be determined by appropriate RET measurements. However, to get reliable results, one should approach the conditions of the intended measurement (setup and current levels) as close as possible. This will lead to very time-consuming studies. Furthermore, even if one uses exactly the conditions of the current measurement (just with half of the input coil turns reversed to obtain an RET setup), there still remains a hard-to-quantify uncertainty contribution from the fact that the coupling of wideband noise to the SQUID crucially depends on how combined CCC windings are composed.

The ULCA is a powerful and flexible tool for the measurement or generation of small electric currents as well as for the calibration of high-value resistors [21]. Combined with a suitable CCC for traceable calibration, it allows substantially improved uncertainties at low currents. Compared with the current amplification with CCC alone, the ULCA offers better noise performance at low frequencies and avoids the systematic uncertainties that appear at low currents due to noise rectification in the SQUID. The ULCA considerably benefits from the availability of the new 14-bit CCC. Compared with the 12-bit CCC, the four times larger flux at given current level results in a correspondingly reduced calibration uncertainty

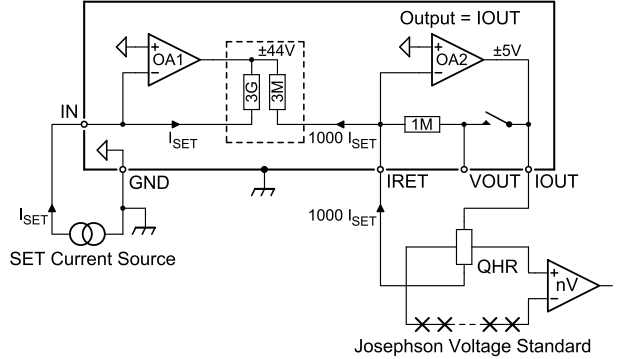


Fig. 9. Quantum metrology triangle experiment with the ULCA amplifying the SET-generated current. The current gain is calibrated with a CCC. The positive input of the nanovoltmeter is connected to the low-voltage side (near ground potential) of the QHR. For simplicity, the screens around SET current source, QHR, Josephson voltage standard, and nanovoltmeter are omitted.

contribution caused by noise rectification. For the same reason, the 14-bit CCC allows verification of the ULCA's linearity down to lower current levels than the 12-bit CCC.

The methods currently used at NMIs for picoammeter calibrations in the sub-nanoampere regime allow uncertainties of about 10 ppm at best [6]–[12]; about 1 ppm at 100 pA was obtained with a special setup based on a 1-G $\Omega$  resistor calibrated with a CCC [1]. As the ULCA can be configured for current sourcing [21], it might be an improved alternative. Compared with the capacitor charging method, the ULCA concept avoids the limiting uncertainty contribution from the frequency dependence of the capacitance [32], and furthermore allows the generation of arbitrary wave forms. At low currents, the overall uncertainty is usually dominated by noise. Therefore, we are currently developing a ULCA variant with a reduced noise level of  $0.8 \text{ fA}/\sqrt{\text{Hz}}$  and an increased transresistance of  $A_{TR} = 10 \text{ G}\Omega$ . As this noise level is comparable with that of commercial picoammeters in the lowest current ranges, we do not expect an unacceptable contribution of the ULCA's noise for calibrations in the sub-picoampere regime.

The superior ULCA performance not only offers benefits for calibration applications, but also has implications for fundamental metrology research. For the development of SET devices generating currents of the order of 100 pA it becomes increasingly important to accurately measure their current–voltage characteristics in order to predict the achievable uncertainty on the basis of theoretical models (see [35], [36], and the references herein). The handy ULCA is well suited for such measurements, allowing ppm accuracy at current levels of 100 pA within acceptable averaging times.

Finally, the ULCA in combination with the 14-bit CCC is also a promising candidate for the realization of a quantum metrology triangle experiment [37]. The straightforward method would be to pass the current from the SET device into a ULCA with *voltage output* that is calibrated against the QHR, and to measure the signal at the ULCA output with a high-accuracy voltmeter calibrated with a Josephson voltage standard. Fig. 9 shows an alternative approach, where the current from the SET device is measured with a ULCA

in the *current output* mode, i.e., with the QHR directly used for  $R_{\text{ext}}$ . This scheme avoids the uncertainty contribution from the standard resistor in the ULCA's output stage. The voltage across the QHR, 1.29 mV for 100 pA from the SET device, is compared with a matched voltage from a Josephson voltage standard using a nanovoltmeter as the null detector (for example, the device in [38] exhibits a white noise level of 0.73 nV/ $\sqrt{\text{Hz}}$  down to below 10 mHz and does therefore not noticeably contribute to the overall uncertainty in the proposed setup). In Fig. 9, the ULCA is acting as a 1000:1 CCC with a superior low-frequency noise performance compared with existing CCCs. Short-term drifts in the current gain  $G_I$  can be suppressed by using two separate ULCA instruments alternately, one of which measures the SET current while the other is calibrated with the CCC. Hereby, the total measurement time can be extended considerably without increasing the uncertainty contribution caused by the limited stability of the ULCA's current gain. Within an averaging time of about one day, an uncertainty of 0.1 ppm seems achievable for the measurement of a 100-pA direct current.

**Note Added in Proof:** The short between the 2-turn winding and one of the 1024-turn windings of our 14-bit CCC was caused by poor isolation in the wiring between the cryogenic part and room temperature. We were able to fix the problem by using a spare wire pair for the 2-turn winding.

#### ACKNOWLEDGMENT

The authors would like to thank R. Behr, M. Fleischer-Bartsch, S. Gruber, C. Krause, G. Muchow, M. Piepenhagen, B. Schumacher, and G.-D. Willenberg for their valuable contributions.

#### REFERENCES

- [1] S. P. Giblin *et al.*, "Towards a quantum representation of the ampere using single electron pumps," *Nature Commun.*, vol. 3, Jul. 2012, Art. ID 930.
- [2] J. P. Pekola *et al.*, "Single-electron current sources: Toward a refined definition of the ampere," *Rev. Modern Phys.*, vol. 85, no. 4, pp. 1421–1472, Oct. 2013.
- [3] L. Fricke *et al.*, "Self-referenced single-electron quantized current source," *Phys. Rev. Lett.*, vol. 112, no. 22, p. 226803, Jun. 2014.
- [4] M.-H. Bae *et al.*, "Precision measurement of a potential-profile tunable single-electron pump," *Metrologia*, vol. 52, no. 2, pp. 195–200, Apr. 2015.
- [5] *Mise en Pratique for the Ampere and Other Electric Units in the International System of Units (SI)*, CCEM Working Group on the SI, document CCEM/09-05, 2009. [Online]. Available: <http://www.bipm.org/cce/CCEM/Allowed/26/CCEM-09-05.pdf>
- [6] G.-D. Willenberg, "EUROMET-EM-S24: Supplementary comparison of small current sources," *Metrologia*, vol. 50, no. 1A, p. 01002, 2013.
- [7] G.-D. Willenberg, H. N. Tauscher, and P. Warnecke, "A traceable precision current source for currents between 100 aA and 10 pA," *IEEE Trans. Instrum. Meas.*, vol. 52, no. 2, pp. 436–439, Apr. 2003.
- [8] H. E. van den Brom, P. de la Court, and G. Rietveld, "Accurate subpicoampere current source based on a differentiating capacitor with software-controlled nonlinearity compensation," *IEEE Trans. Instrum. Meas.*, vol. 54, no. 2, pp. 554–558, Apr. 2005.
- [9] L. Callegaro, V. D'Elia, P. P. Capra, and A. Sosso, "Techniques for traceable measurements of small currents," *IEEE Trans. Instrum. Meas.*, vol. 56, no. 2, pp. 295–299, Apr. 2007.
- [10] N. E. Fletcher, S. P. Giblin, J. M. Williams, and K. J. Lines, "New capability for generating and measuring small DC currents at NPL," *IEEE Trans. Instrum. Meas.*, vol. 56, no. 2, pp. 326–330, Apr. 2007.
- [11] T. Bergsten, K.-E. Rydler, O. Gunnarsson, G. Eklund, and V. Tarasso, "A precision current source using  $\Delta - \Sigma$  modulation," *IEEE Trans. Instrum. Meas.*, vol. 60, no. 7, pp. 2341–2346, Jul. 2011.
- [12] BIPM. (2014). *Calibration and Measurement Capabilities Electricity and Magnetism*. [Online]. Available: [http://kcdb.bipm.org/AppendixC/country\\_list.asp?Sservice=EM/DC.3.2](http://kcdb.bipm.org/AppendixC/country_list.asp?Sservice=EM/DC.3.2)
- [13] H. Scherer, S. P. Giblin, X. Jehl, A. Manninen, F. Piquemal, and D. A. Ritchie, "Introducing joint research project 'quantum ampere' for the realisation of the new SI ampere," in *Proc. EPJ Web Conf.*, vol. 77, 2014, p. 00004. [Online]. Available: [http://epjwoc.epj.org/articles/epjconf/abs/2014/14/epjconf\\_icm2014\\_00004/epjconf\\_icm2014\\_00004.html](http://epjwoc.epj.org/articles/epjconf/abs/2014/14/epjconf_icm2014_00004/epjconf_icm2014_00004.html)
- [14] I. K. Harvey, "A precise low temperature dc ratio transformer," *Rev. Sci. Instrum.*, vol. 43, no. 11, pp. 1626–1629, Nov. 1972.
- [15] D. B. Sullivan and R. F. Dziuba, "Low temperature direct current comparator," *Rev. Sci. Instrum.*, vol. 45, no. 4, pp. 517–519, Apr. 1974.
- [16] F. Gay, F. Piquemal, and G. Genève, "Ultralow noise current amplifier based on a cryogenic current comparator," *Rev. Sci. Instrum.*, vol. 71, no. 12, pp. 4592–4595, Dec. 2000.
- [17] E. Bartolomé, "Cryogenic current comparators with optimum SQUID readout for current and resistance quantum metrology," Ph.D. dissertation, Dept. Appl. Phys., Univ. Twente, Enschede, The Netherlands, 2002.
- [18] F. Rengnez, O. Séron, L. Devoille, D. Placko, and F. Piquemal, "A femto ampere current amplifier based on a 30 000:1 cryogenic current comparator," in *29th Conf. Precis. Electromagn. Meas. Dig.*, Rio de Janeiro, Brazil, Aug. 2014, pp. 296–297.
- [19] M. Götz, E. Pesel, and D. Drung, "A compact 14-bit cryogenic current comparator," in *29th Conf. Precis. Electromagn. Meas. Dig.*, Rio de Janeiro, Brazil, Aug. 2014, pp. 684–685.
- [20] D. Drung, C. Krause, U. Becker, H. Scherer, and F. J. Ahlers, "Ultra-stable low-noise current amplifier," in *29th Conf. Precis. Electromagn. Meas. Dig.*, Rio de Janeiro, Brazil, Aug. 2014, pp. 656–657.
- [21] D. Drung, C. Krause, U. Becker, H. Scherer, and F. J. Ahlers, "Ultra-stable low-noise current amplifier: A novel device for measuring small electric currents with high accuracy," *Rev. Sci. Instrum.*, vol. 86, no. 2, p. 024703, Feb. 2015.
- [22] M. Götz *et al.*, "Improved cryogenic current comparator setup with digital current sources," *IEEE Trans. Instrum. Meas.*, vol. 58, no. 4, pp. 1176–1182, Apr. 2009.
- [23] J. Gallop and F. Piquemal, "SQUIDs for standards and metrology," in *The SQUID Handbook: Applications of SQUIDs and SQUID Systems*, vol. 2, J. Clarke and A. I. Braginski, Eds. Weinheim, Germany: Wiley, 2006, pp. 101–114.
- [24] D. Drung *et al.*, "Improving the stability of cryogenic current comparator setups," *Supercond. Sci. Technol.*, vol. 22, no. 11, p. 114004, Nov. 2009.
- [25] F. Delahaye and B. Jeckelmann, "Revised technical guidelines for reliable dc measurements of the quantized Hall resistance," *Metrologia*, vol. 40, no. 5, pp. 217–223, Oct. 2003.
- [26] M. Götz, D. Drung, E. Pesel, and F.-J. Ahlers, "Settling behavior of the bridge voltage in resistance ratio measurements with cryogenic current comparators," *IEEE Trans. Instrum. Meas.*, vol. 60, no. 7, pp. 2660–2666, Jul. 2011.
- [27] R. Goebel, N. Fletcher, B. Rolland, M. Götz, and E. Pesel, "Final report on the on-going comparison BIPM.EM-K12: Comparison of quantum Hall effect resistance standards of the PTB and the BIPM," *Metrologia*, vol. 51, p. 01011, Jul. 2014.
- [28] D. Drung, J. Beyer, M. Peters, J.-H. Storm, and T. Schurig, "Novel SQUID current sensors with high linearity at high frequencies," *IEEE Trans. Appl. Supercond.*, vol. 19, no. 3, pp. 772–777, Jun. 2009.
- [29] D. Drung *et al.*, "Highly sensitive and easy-to-use SQUID sensors," *IEEE Trans. Appl. Supercond.*, vol. 17, no. 2, pp. 699–704, Jun. 2007.
- [30] F. J. Ahlers, M. Götz, and D. Drung, "Identification and correction of slowly decaying transients in measurements with periodic bias reversal," in *29th Conf. Precis. Electromagn. Meas. Dig.*, Rio de Janeiro, Brazil, Aug. 2014, pp. 292–293.
- [31] D. Drung, M. Götz, E. Pesel, H.-J. Barthelmess, and C. Hinrichs, "Aspects of application and calibration of a binary compensation unit for cryogenic current comparator setups," *IEEE Trans. Instrum. Meas.*, vol. 62, no. 10, pp. 2820–2827, Oct. 2013.
- [32] S. P. Giblin, G.-D. Willenberg, and N. E. Fletcher, "Frequency dependence of gas-dielectric capacitors used in sub-nA-reference current generators," in *27th Conf. Precis. Electromagn. Meas. Dig.*, Daejeon, Korea, Jun. 2010, pp. 318–319.

- [33] H. Scherer, G.-D. Willenberg, D. Drung, M. Götz, and E. Pesel, "Traceable precision generation and measurement of pA direct currents," in *29th Conf. Precis. Electromagn. Meas. Dig.*, Rio de Janeiro, Brazil, Aug. 2014, pp. 550–551.
- [34] G.-D. Willenberg and N. H. Tauscher, "Novel digital voltage ramp generator for use in precision current sources in the picoampere range," *IEEE Trans. Instrum. Meas.*, vol. 58, no. 4, pp. 756–760, Apr. 2009.
- [35] V. Kashcheyevs and J. Timoshenko, "Quantum fluctuations and coherence in high-precision single-electron capture," *Phys. Rev. Lett.*, vol. 109, no. 21, p. 216801, Nov. 2012.
- [36] V. Kashcheyevs and J. Timoshenko, "Modeling of a tunable-barrier non-adiabatic electron pump beyond the decay cascade model," in *29th Conf. Precis. Electromagn. Meas. Dig.*, Rio de Janeiro, Brazil, Aug. 2014, pp. 536–537.
- [37] H. Scherer and B. Camarota, "Quantum metrology triangle experiments: A status review," *Meas. Sci. Technol.*, vol. 23, no. 12, p. 124010, Dec. 2012.
- [38] D. Drung and J.-H. Storm, "Ultralow-noise chopper amplifier with low input charge injection," *IEEE Trans. Instrum. Meas.*, vol. 60, no. 7, pp. 2347–2352, Jul. 2011.



**Dietmar Drung** was born in Mühlacker, Germany, in 1958. He received the Dipl.-Ing. and Dr.-Ing. degrees in electrical engineering from the University of Karlsruhe, Karlsruhe, Germany, in 1982 and 1988, respectively.

He was a Researcher with the University of Karlsruhe from 1983 to 1988. In 1988, he joined Physikalisch-Technische Bundesanstalt, Berlin, Germany, where he has been involved in superconducting quantum interference devices (SQUIDs) and SQUID readout electronics.

In 2009, he became a Senior Scientist in superconducting sensors. His current research interests include the development of low-noise amplifiers and measurement systems for magnetic sensing and electrical metrology.



**Martin Götz** was born in Erfurt, Germany, in 1968. He received the Diploma and Ph.D. degrees in physics from Friedrich Schiller University, Jena, Germany, in 1992 and 1997, respectively.

He has been with Physikalisch-Technische Bundesanstalt, Braunschweig, Germany, since 1999. His current research interests include the further improvement of cryogenic current comparator-based setups and applications of the quantum Hall effect in electrical metrology.



**Eckart Pesel** was born in Uelzen, Germany, in 1960. He received the Dipl.-Ing. degree from Fachhochschule Wolfenbüttel, Wolfenbüttel, Germany, in 1990.

He has been with Physikalisch-Technische Bundesanstalt, Braunschweig, Germany, since 1990, where he is involved in the quantum Hall effect and the development of the cryogenic current comparator.



**Hansjörg Scherer** was born in Germany in 1965. He received the Diploma and Ph.D. degrees in physics from the Technical University of Braunschweig, Braunschweig, Germany, in 1992 and 1995, respectively.

He joined Physikalisch-Technische Bundesanstalt, Braunschweig, in 1992, where he has been involved in single-electron tunneling since 1995. He is currently the Head of the working group in the field of single-electron tunneling, electrical current, and charge. His current research interests include quantum electronics and quantum metrology.